Engineering Notes

ENGINEERING NOTES are short manuscripts describing new developments or important results of a preliminary nature. These Notes cannot exceed 6 manuscript pages and 3 figures; a page of text may be substituted for a figure and vice versa. After informal review by the editors, they may be published within a few months of the date of receipt. Style requirements are the same as for regular contributions (see inside back cover).

AIAA 82-4041

Approximate Calculation of Aerodynamic Coefficients for Rotating Slender Bodies at 90 deg Incidence

Takashi Yoshinaga,* Atsushi Tate,† and Kenji Inoue‡
National Aerospace Laboratory, Chofu, Tokyo, Japan

Introduction

In recent years, the side force acting on slender bodies of revolution at high incidence has received a great deal of attention because it often causes rockets and aircraft to become uncontrollable. Drop tests of sounding rocket head models showed that, after some initial tumbling motions, most of them dropped, rotating in a plane parallel to the sea surface like propellers (flat spin).[1,2] If the rotation rate is high, the motion might damage the body or its payload. Although much work concerning the side force acting on a body at incidence has been published,[3] there are few theoretical or semiempirical methods available to estimate the aerodynamic coefficients for such rotating slender bodies at high incidence.

The present paper presents a simple method used to predict the aerodynamic coefficients of a slender body rotating by the side force near the critical Reynolds number at an angle of attack of 90 deg. From the results, the steady rotation rate of the flat spin is estimated and compared with experimental data of other authors.

Analysis

Allen and Perkins[4] and Jorgensen[5] have given methods to predict the aerodynamic coefficients for a nonrotating body at incidence. The present method is based on the experimental observation that crossflow is predominant on the fore side of a slender body at high incidence[3,4] and distinct lift (side force $C_L \simeq 1$) acts within a narrow range of Reynolds number.[6,7] The present calculations employ a method similar to the simple blade element theory of propellers. The translational motion of the body is not considered.

Figure 1 is the sketch of a slender body of length l at incidence 90 deg and of its small element on which the drag and the lift act. It is assumed that the body is rotating at the rate of ϕ' around an axis passing through the center of gravity at x_g. Since the element at station x has the circumferential velocity $\phi'|x-x_g|$ owing to the rotation, the flow past the element has the net velocity V, the vector sum of freestream velocity V_∞ and $\phi'|x-x_g|$. The elemental lift and drag force are taken to be perpendicular and parallel, respectively, to the velocity vector V. The elemental normal force dN, the elemental side force dY, and the elemental yawing moment dn, caused by dY around the center of gravity, are as follows

$$dN = \tfrac{1}{2}\rho V^2 D(x)\,(C_L \sin\gamma + C_D \cos\gamma)\,dx \tag{1}$$

$$dY = \tfrac{1}{2}\rho V^2 D(x)\,(C_L \cos\gamma - C_D \sin\gamma)\,dx \tag{2}$$

$$dn = \tfrac{1}{2}\rho V^2 D(x)\,|x-x_g|\,(C_L \cos\gamma - C_D \sin\gamma)\,dx \tag{3}$$

where C_L and C_D are the lift and drag coefficients for a two-dimensional circular cylinder, ρ the density of air, $D(x)$ the body diameter, and γ the angle defined by

$$\gamma = \tan^{-1} |x-x_g|\phi'/V_\infty \tag{4}$$

Integrating Eqs. (1-3) from 0 to l yields the net normal force N, the side force Y, and the yawing moment n. Introducing nondimensional coefficients, length and angular velocity by

$$C_N = \frac{N}{\tfrac{1}{2}\rho V_\infty^2 S}, \qquad C_Y = \frac{Y}{\tfrac{1}{2}\rho V_\infty^2 S}, \qquad C_n = \frac{n}{\tfrac{1}{2}\rho V_\infty^2 S \cdot D_0}$$

$$\bar{x} = \frac{x}{D_0}, \qquad \bar{D}(\bar{x}) = \frac{D(\bar{x})}{D_0}, \qquad \dot{\phi} = \frac{\phi' D_0}{V_\infty}$$

where $S = (\pi/4)D_0^2$ and D_0 is the maximum diameter, we get the nondimensional expressions as

$$C_N = \eta \frac{4}{\pi} \int_0^{l/D_0} \bar{D}(\bar{x})\,(1+\dot{\phi}^2 |\bar{x}-\bar{x}_g|^2)^{1/2} \times (C_L \dot{\phi} |\bar{x}-\bar{x}_g| + C_D)\,d\bar{x} \tag{5}$$

$$C_Y = \frac{4}{\pi} \int_0^{l/D_0} \bar{D}(\bar{x})\,(1+\dot{\phi}^2 |\bar{x}-\bar{x}_g|^2)^{1/2} \times (C_L - C_D \dot{\phi} |\bar{x}-\bar{x}_g|)\,d\bar{x} \tag{6}$$

$$C_n = \frac{4}{\pi} \int_0^{l/D_0} \bar{D}(\bar{x})\,|\bar{x}-\bar{x}_g|\,(1+\dot{\phi}^2 |\bar{x}-\bar{x}_g|^2)^{1/2} \times (C_L - C_D \dot{\phi} |\bar{x}-\bar{x}_g|)\,d\bar{x} \tag{7}$$

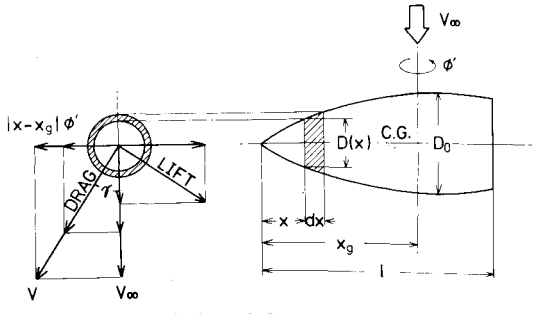

Fig. 1 Schematic description of elemental flowfield and coordinates system.

Received April 6, 1981; revision received Aug. 13, 1981.

*Head, Aerothermodynamics Section, First Aerodynamics Division. Member AIAA.
†Research Official, Aerothermodynamics Section, First Aerodynamics Division.
‡Head, Boundary Layer Research Section, First Aerodynamics Division. Member AIAA.

where η is the correction factor for the body of finite length.[4] Dividing C_n by C_Y, a nondimensional distance between the center of gravity and the center of side force is obtained. In this calculation, the direction of the lift force on both sides of the axis is selected so as to give the same direction of moment.

To calculate integrals in the above equations numerically, C_L and C_D at each element of the body must be given as functions of the local Reynolds number. Experimental results on a circular cylinder near the critical Reynolds number show that there are two critical Reynolds numbers, the lower one Re_{c1} and the higher one Re_{c2} when the freestream velocity increases. At these Reynolds numbers, the drag and lift coefficients vary stepwise since bubble formation occurs abruptly at these values.[7] The fact that lift acts between the two critical Reynolds numbers is the key to calculating the coefficients. In the present calculation, the following values based on experimental results[5,7] were used

$$Re<Re_{c1}, \quad C_L=0, \quad C_D=1$$

$$Re_{c1}<Re<Re_{c2}, \quad C_L=1, \quad C_D=0.4$$

$$Re_{c2}<Re<Re_3, \quad C_L=0, \quad C_D=0.2$$

$$Re_3<Re \quad C_L=0 \quad C_D=0.332\log_{10}Re-1.80$$

$$Re_{c1}=3.7\times10^5 \ (3.5\times10^5), \quad Re_{c2}=3.9\times10^5 \ (3.7\times10^5)$$

$$Re_3=10^6$$

When the total rotating moment due to the lift balances with the total impeding moment due to the drag, the body rotates at a constant angular velocity (steady rotation). To calculate the constant angular velocity at a given freestream velocity, the value of $\dot{\phi}$ for which $C_n=0$ must be found. Substituting $\dot{\phi}$ into Eqs. (5) and (6), the normal force and side force coefficients for the condition are obtained.

Results and Discussion

Figure 2 shows the variation of the steady rotation rate N_r as functions of freestream velocity for a circular cylinder of finite length and also for a blunted cone cylinder. It also includes the experimental data recently obtained by Kubota et al.[8] for the same bodies.

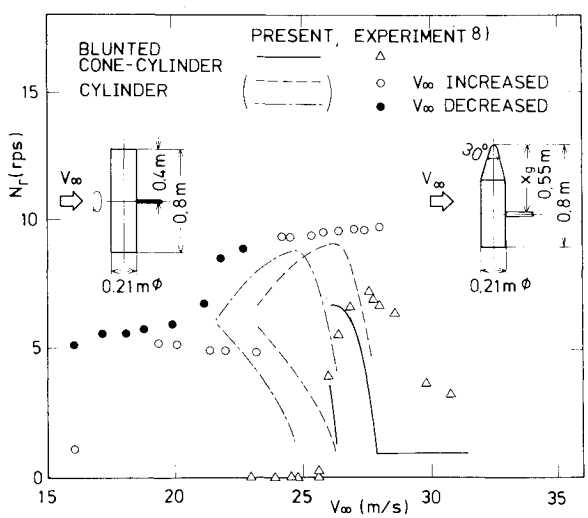

Fig. 2 Steady flat spin rotation rates for bodies as functions of freestream velocity (present theory, —— blunted cone cylinder, nose angle 30 deg, $Re_{c1}=3.7\times10^5$, $Re_{c2}=3.9\times10^5$; ---- cylinder, $Re_{c1}=3.7\times10^5$, $Re_{c2}=3.9\times10^5$; – – – cylinder, $Re_{c1}=3.5\times10^5$, $Re_{c2}=3.7\times10^5$).

The present theory shows that the circular cylinder can rotate at a freestream velocity that is less than that given by the lower critical Reynolds number Re_{c1}, because somewhere on the cylinder the local resultant velocity exceeds the critical velocity, causing the yawing moment to act. There are two values of rotation rate at which the yawing moment C_n becomes zero. This means that if the cylindrical body is rotated up to the rate of the lower curve by some mechanism, the rotation is accelerated up to the higher curve, because between the two values the total yawing moment n is positive. The experimental data show that the body begins to rotate at a freestream velocity somewhat lower than that predicted by the present theory. Probably this is the result of the three-dimensional effect of the flow about the cylinder. The abrupt increase in the rotation rate up to about 9 rps at the freestream velocity of 24 m/s, seems to correspond to the theoretical results mentioned above. The maximum rotation rate predicted by the present theory agrees well with the results of the experiments. The theory predicts that as the freestream Reynolds number Re_∞ $(=D_0V_\infty/\nu)$ approaches the higher critical value Re_{c2}, the rotation rate decreases and the value becomes zero at Re_{c2}. In the experiment, on the other hand, the model continues to rotate at Reynolds number higher than Re_{c2}. In the case of a cylinder, the integrals in Eqs. (5-7) are obtained analytically.

Next, the present method is applied to a cone cylinder. The theory predicts that the model continues to rotate at a Reynolds number lower than the critical value by the same reason as that for a cylinder of finite length. However, differing from the cylinder, the calculation shows that the cone cylinder continues to rotate even beyond the critical Reynolds number based on maximum body diameter, since somewhere on the nose section the local Reynolds number, based on the local diameter, is within the critical range of the Reynolds number. Experimental results show that near the critical Reynolds number, the body whose center of gravity is about 0.55 m from the nose rotates at the approximate maximum rotation rate predicted by the theory. At the Reynolds number exceeding the critical value, the theoretical rotation rates are far less than the experimental results. Recently, Kamiya et al.[9] have shown that another side force acting near the shoulder of a cone cylinder appears beyond the critical Reynolds number and have attributed such a high rotation rate to it.

Although calculated results are not shown here, the steady rotation rate decreases remarkably for a longer body, because the impeding moment due to the drag force becomes greater for a longer body.

Finally, a cylinder forced to rotate at constant rates at fixed freestream velocities is considered. In Fig. 3, drag coefficients

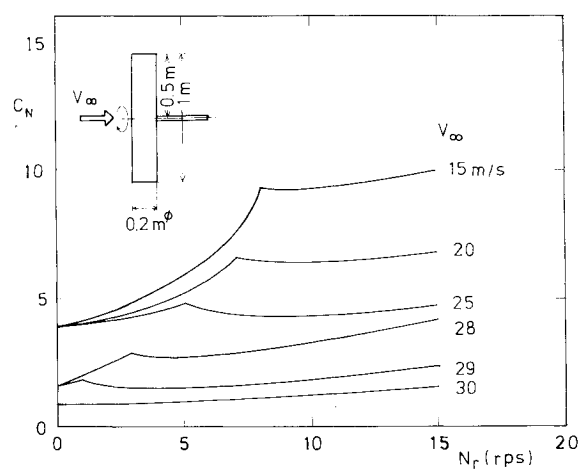

Fig. 3 Normal force coefficients of a circular cylinder of finite length (diam 0.2 m, length 1 m, $\eta=0.63$ in Eq. (5); for $V_\infty=30$ m/s, $Re_\infty\simeq4.2\times10^5>Re_{c2}$).

for a rotating cylinder evaluated by Eq. (5) are depicted as functions of rotation rate. When $Re_\infty > Re_{c2}$, normal force (or drag) coefficient C_N increases monotonically as the Reynolds number increases. (Figure 3 shows the case for $V_\infty = 30$ m/s.) This will explain why the drag force on a rotating body in the drop test is greater than that on the model at rest in the wind tunnel test.[2]

In view of the rough approximate analysis, qualitative agreement with the experimental data is encouraging as a method to predict the maximum rotation rates near critical Reynolds number.

From the practical point of view, the flat spin will be prevented by making the boundary layer on the whole surface of the body turbulent with artificial roughness elements such as tripping wires.[10]

References

[1] Kubota, H., private communication, Nov. 1978.

[2] Shirouzu, M., Kubota, H., and Shibato, Y., "Aerodynamic Aspects on Recovery of Sounding Rocket Payload," Paper IAF-80E 214 presented at XXXI Congress of International Astronautical Federation, Sept. 1980.

[3] Ericsson, L.E. and Reding, J.P., "Steady and Unsteady Vortex-Induced Asymmetric Loads on Slender Vehicles," *Journal of Spacecraft and Rockets*, Vol. 18, March-April 1981, pp. 97-109.

[4] Allen, H.J. and Perkins, E.W., "Characteristics of Flow over Inclined Bodies of Revolution," NACA RM A50L07, 1951.

[5] Jorgensen, L.H., "Prediction of Static Aerodynamic Characteristics for Space-Shuttle-Like and Other Bodies at Angles of Attack from 0° to 180°," NASA TN D-6996, Jan. 1973.

[6] Bearman, P.W., "On Vortex Shedding from a Circular Cylinder in the Critical Reynolds Number Regime," *Journal of Fluid Mechanics*, Vol. 37, July 1969, pp. 577-585.

[7] Kamiya, N., Suzuki, S., and Nishi, T., "On the Aerodynamic Force Acting on a Circular Cylinder in the Critical Range of the Reynolds Number," AIAA Paper 79-1475, July 1979.

[8] Kubota, H., Arai, I., and Matsuzaka, M., "Wind Tunnel Investigations for the Flat Spin of Slender Bodies at High Angles of Attack," Paper 82-0054 to be presented at the AIAA 20th Aerospace Sciences Meeting, Orlando, Fla., Jan. 1982.

[9] Kamiya, N., Suzuki, S., Nakamura, M., and Yoshinaga, T., "Some Practical Aspects of the Burst of Laminar Separation Bubbles," Paper ICAS-80-10 presented at the 12th Congress of the International Council of the Aeronautical Sciences, Oct. 1980.

[10] Pick, G.S., "Investigation of Side Forces on Ogive-Cylinder Bodies at High Angles of Attack in the M = 0.5 to 1.1 Range," AIAA Paper 71-570, June 1971.

AIAA 82-4042

Subsonic and Transonic Roll Damping Measurements on Basic Finner

H. Sundara Murthy*
National Aeronautical Laboratory, Bangalore, India

Nomenclature

C_l = rolling moment/$q_\infty Sd$, rolling moment coefficient
C_{l_p} = $\partial C_l / \partial (pd/2V_\infty)$, roll damping coefficient
d = body diameter
M_∞ = freestream Mach number
p = roll rate, rad/s
q_∞ = freestream dynamic pressure
Re_d = Reynolds number based on body diameter
S = $\pi d^2/4$, reference area
V_∞ = freestream velocity

Received April 17, 1981; revision received Aug. 19, 1981.

*Scientist, Aerodynamics Division.

Introduction

DEVELOPMENT of new test techniques and prediction methods for aerodynamic coefficient estimation to meet the increasing needs of industry is a well-known feature of aerospace research and development. It is general practice to validate these new methods by generating data and comparing them with other available results on a widely accepted configuration—the so-called calibration model. It is reported[1] that the Basic Finner (Fig. 1) has been selected as a standard configuration for this purpose by the Supersonic Tunnel Association and AGARD. Consequent to this, experimental results of aerodynamic coefficients on this configuration is obviously of general interest. To fulfill this need, Ref. 1 presented wind-tunnel measured pitch damping and stiffness coefficients on the Basic Finner at $M_\infty = 1.5$.

Measurements of roll damping coefficient on the Basic Finner are reported in Refs. 2-4. These measurements covered the supersonic speed range. Excepting $M_\infty = 0.22$ and 0.77, there does not seem to be any published test data on this configuration at subsonic and transonic speeds. This Note presents wind-tunnel roll damping data on the Basic Finner in

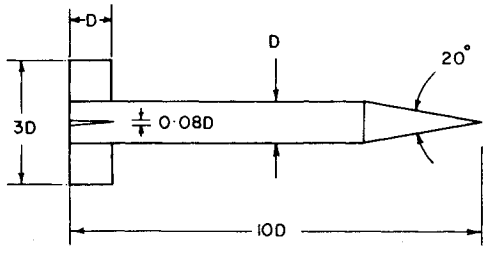

Fig. 1 Basic Finner model.

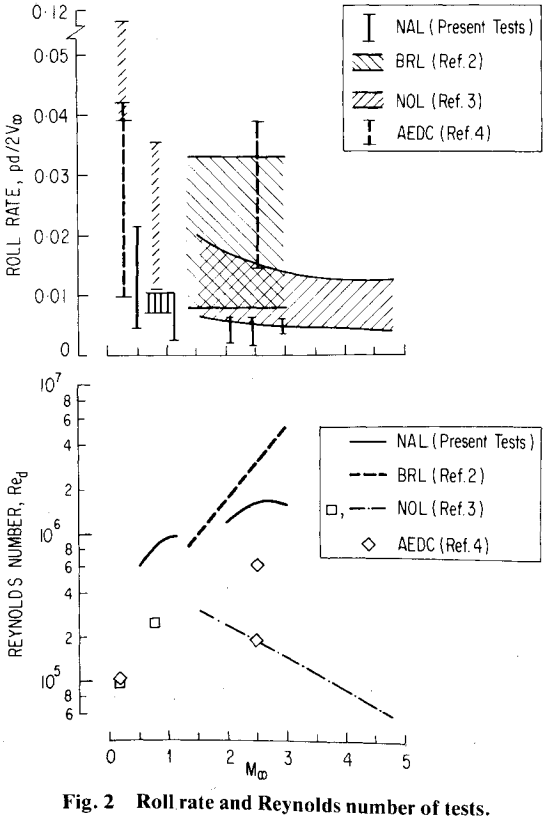

Fig. 2 Roll rate and Reynolds number of tests.